Fatigue Crack Growth Behavior and Associated Microstructure in a Metastable High-Entropy Alloy

As Published: 10.1016/J.PROSTR.2018.12.159

Publisher: Elsevier BV

Persistent URL: https://hdl.handle.net/1721.1/135054

Version: Final published version: final published article, as it appeared in a journal, conference proceedings, or other formally published context

Available online at www.sciencedirect.com

ScienceDirect

Procedia Structural Integrity 13 (2018) 831–836

Structural Integrity Procedia

www.elsevier.com/locate/procedia

ECF22 - Loading and Environmental effects on Structural Integrity

Fatigue Crack Growth Behavior and Associated Microstructure in a Metastable High-Entropy Alloy

Takeshi Eguchi[a,*], Motomichi Koyama[a], Yoshihiro Fukushima[a], Cemal Cem Tasan[b], Kaneaki Tsuzaki[a]

[a]*Department of Mechanical Engineering, Kyushu University, Motooka 744, Nishi-ku, Fukuoka 819-0395, Japan*
[b]*Department of Materials Science and Engineering, Massachusettes Institute of Technology, 77 Massachusettes Avenue, Cambridge, MA 02139, USA*

Abstract

High-entropy alloys (HEAs) containing different kinds of high-concentration solute atoms provide new concepts for obtaining excellent balance of strength and ductility. In particular, a metastable dual-phase HEA (Fe30Mn10Cr10Co; FCC matrix and HCP second phase) shows superior ductility and strength owing to the transformation-induced plasticity effect associated with deformation-induced HCP-martensitic transformation. In this context, the fatigue properties of metastable HEAs are to be investigated towards practical applications as structure materials. In this study, the fatigue crack growth behaviors of HEA and type 316L austenitic stainless steel (FCC single phase) were comparatively examined. The crack growth rate of HEA was comparable to that of 316L. In HEA, the fatigue crack was covered by a large amount of HCP-martensite. In general, the HCP-martensite was cracked easily because of the smaller number of slip systems. However, the negative effect of HCP-martensite did not appear in the fatigue crack growth rate of HEA. By electron channeling contrast imaging, we found that the HCP-martensite beneath the fracture surface contained significant orientation gradient and high density of dislocations, indicating that HCP-martensite in the present Fe30Mn10Cr10Co HEA had high plastic deformability and associated stress accommodation capacity.

Peer-review under responsibility of the ECF22 organizers.

Keywords: High-entropy alloy; HCP-martensite; Fatigue; Crack growth behavior.

* Corresponding author. Tel.: +81-92-802-3288.
E-mail address: 2TE17803T@s.kyushu-u.ac.jp

2452-3216
Peer-review under responsibility of the ECF22 organizers.
10.1016/j.prostr.2018.12.159

1. Introduction

Deformation-induced HCP-martensitic transformation in high-entropy alloy (HEA) has been reported to overcome the strength-ductility balance unlike conventional stable austenitic steels such as type 316L stainless steel (Li et al., 2016). In particular, the dislocation motion is inhibited at the FCC/HCP interface, which realizes high work hardening capacity. Accordingly, the sustained high work hardening capacity results in superior uniform elongation.

However, when HCP-martensite is utilized, we must note damage accumulation behavior at the microstructural interface because damage accumulation plays ambivalent roles on ductility (Koyama et al., 2008). More specifically, the accumulation of damage such as dislocations at microstructural interfaces results in work hardening and enhanced uniform elongation, while damage accumulation may cause vacancy and micro-void formations at the interface, deteriorating the limit of plastic deformability (Takaki et al., 1990).

In this context, the fatigue problem of metastable HEA is another concern because fatigue is caused by plastic strain evolution at the crack tip. In fact, damage accumulation at a specific microstructural interface accelerates fatigue crack growth (Ju et al., 2017). Therefore, when work hardening is enhanced by the inhibition of dislocation motion at a microstructural interface, the local ductility of the interfacial region must be high enough to avoid the acceleration of fatigue crack propagation. Hence, in this study, we investigated the fatigue crack growth behavior of metastable HEA containing a considerable amount of FCC/HCP interfaces. Furthermore, we present microstructure evolution beneath the fracture surface. More specifically, emphasis is placed on the plasticity of HCP-martensite associated with fatigue crack growth.

2. Experimental procedure

In this study, we prepared Fe30Mn10Cr10Co (at%) HEA. A 50 kg ingot of Fe30Mn10Cr10Co HEA was prepared by vacuum induction melting. The ingot was hot-rolled to 52% thickness at 1273 K, followed by homogenization at 1473 K for 2 h in Ar atmosphere and furnace cooling. The homogenized bar was further hot-rolled to obtain a thickness reduction to 33% (from 60 to 20 mm) at 1273 K. The rolled bar was solution-treated at 1073 K in air for 1 h, followed by water-quenching. The as-solution-treated HEA consisted of metastable austenite matrix and HCP-martensite second phase. We used solution-treated type 316L stainless steel consisting of stable austenite as reference material. The details of the chemical compositions are listed in Table 1.

Tensile specimens were produced by spark machining. Tensile tests were conducted at room temperature, at an initial strain rate of 10^{-4} s^{-1}. Compact tension (CT) specimens were produced in conformity with ASTM standard E647 (ASTM, 2011): their gauge dimensions were 50.8 mm wide, 10 mm thick, and with 10 mm machined-notch-length. The CT specimens were machined using shaper and grinder and the notch was shaped by electric discharge machining. The surfaces of the specimens were then mechanically polished to a mirror finish. The loading axis was parallel to the rolling direction (RD). Fatigue crack growth tests were carried out with constant test load range (ΔP) in the range of stress intensity factor (ΔK) from about 15 to 30 MPa·$m^{1/2}$ at room temperature with constant test frequency f = 1 Hz and constant stress ratio R = 0.1. The test load was varied sinusoidally. A small scale-yielding condition was satisfied under the present conditions.

After fatigue crack growth tests, microstructure observations of HEA were performed by electron back-scatter diffraction (EBSD) analysis and electron channeling contrast imaging (ECCI) after cutting the specimens through the middle of the CT specimen thickness and then mechanically polishing them with colloidal silica to remove damaged layers. EBSD analysis was performed at 20 kV with beam step size 50 nm or 170 nm. ECCI was performed at 30 kV.

Table 1. Chemical compositions of the alloys (mass %).

Alloys	C	Si	Mn	P	S	N	O	Al	Cr	Co	Ni	Fe
HEA	0.009	–	29.80	0.004	0.007	0.0087	0.015	0.028	9.29	10.46	0.01	50.37
Type 316L	0.012	0.48	0.84	0.027	<0.002	0.033	0.002	0.003	17.9	–	12.1	65.0

3. Results and discussion

3.1. Tensile behavior

The tensile properties are listed in Table 2. HEA showed lower proof stress but higher tensile strength than those of 316L. This was evidently because of deformation-induced HCP-martensitic transformation. As a result, HEA exhibited higher strength-elongation (σ_B-ε_u) balance than that of 316L. The superior mechanical characteristics were reported to stem from a combined effect of high configurational entropy and transformation-induced plasticity (TRIP) (Li et al., 2017). In particular, the TRIP effect was associated with the deformation-induced HCP-martensitic transformation. The primary factor causing high work hardening was dynamic strain partitioning associated with the formation of FCC/HCP interfaces. An effect of damage accumulation at the interface on fatigue crack growth was our concern, as described in the introduction. In this context, we must note that the fracture surface of HEA had dimples as a predominant feature (Ichii et al., 2018). Therefore, the local damage resistance at FCC/HCP interface was expected to be high owing to stress accommodation capacity associated with high configurational entropy.

Table 2. Tensile properties of the alloys.

Alloys	0.2% proof stress, $\sigma_{0.2}$ (MPa)	Tensile strength, σ_B (MPa)	Uniform elongation, ε_u (%)	Total elongation, ε_t (%)	$\sigma_B \times \varepsilon_u$ (MPa·%)
HEA	172	733	47.1	53.6	3.45×10^4
316L	250	575	53.9	65.2	3.10×10^4

3.2. Macroscopic features of fatigue crack propagation

Fig. 1 shows the results of fatigue crack growth rate. The crack growth rate of HEA was comparable to that of 316L, even though it was somewhat higher at small ΔK around 18 MPa·m$^{1/2}$. Fig. 2 shows the macroscopic observation results for the fatigue crack propagation path. In optical micrographs (Figs. 2a and 2c), it was seen that fatigue cracks propagated rather smoothly in both the alloys. This indicated that even in HEA, the crack propagated in a mode I type like in 316L, where the main fatigue crack propagated with crack opening, blunting, and re-sharpening processes via alternative slip deformation at the crack tip. It is interesting to note that crack propagation followed a zig-zag fashion in the case of conventional metastable austenitic steels showing deformation-induced HCP-martensitic transformation (Nikulin et al., 2013). For instance, Fe30Mn6Si alloy with FCC/HCP phases showed a zig-zag propagation path because of fracture at FCC/HCP interfaces resulting in the formation of many secondary cracks near the front of the

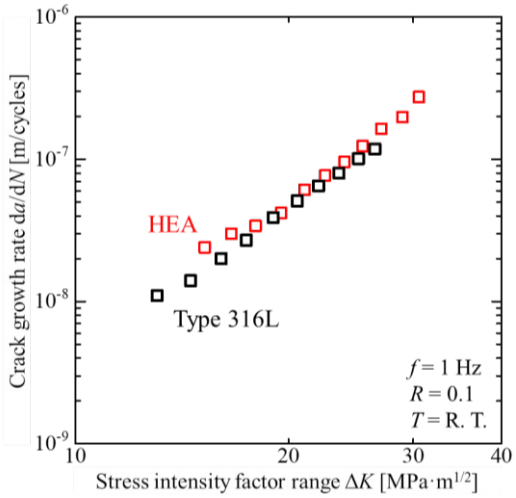

Fig. 1. Crack growth rate plotted against stress intensity factor range.

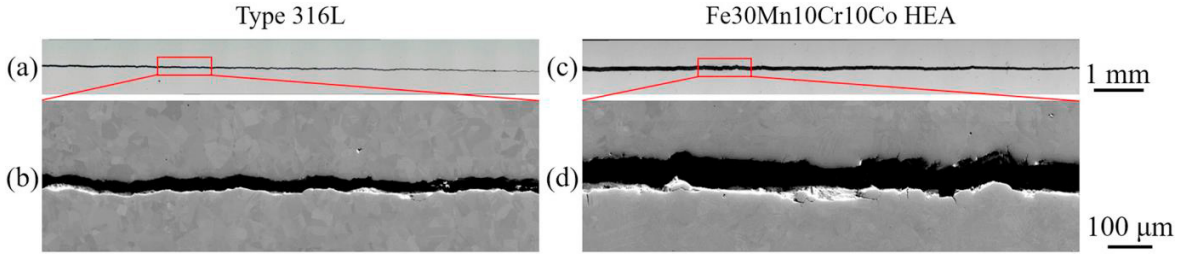

Fig. 2. Macroscopic observation of the fatigue crack propagation paths of 316L and HEA. (a) and (c) show optical microscope images in the range of Δ K of 15–25 MPa·m$^{1/2}$; (b) and (d) show secondary electron images around Δ K of 18 MPa·m$^{1/2}$.

main crack tip, and its crack growth rate became higher than that of Fe30Mn6Al alloy with a stable FCC phase (Ju et al., 2017, Koyama et al., 2018). Secondary cracks were recognized even in HEA, as was seen in the secondary electron image (Fig. 2d). However, secondary cracking was not significant. It was concluded from the comparative study of macroscopic crack propagation behavior that crack propagation of the present HEA with FCC/HCP phases was very similar to that of 316L with stable FCC, and significantly different from that of conventional metastable austenitic steels with deformation-induced HCP-martensitic transformation like the Fe30Mn6Si alloy.

3.3. Microstructure evolution beneath the fracture surface

To clarify the reasons for similarities in macroscopic crack propagation behaviors of HEA and 316L, microstructure observation was done beneath the fracture surface in HEA at relatively low ΔK (18 MPa·m$^{1/2}$) with particular attention to plastic deformability of the HCP phase.

Fig. 3 shows EBSD images beneath the fracture surface of HEA. The fatigue crack of HEA was covered with a large amount of HCP-martensite (Fig. 3a). The thermally-induced HCP-martensite that existed before the fatigue test corresponded to the blocky yellow regions, while the deformation-induced HCP-martensite formed during the fatigue test corresponded to the plate-like regions. It was seen that plate-like HCP-martensite was curved. The grain reference orientation deviation (GROD) mapping in Fig. 3b indicated relatively high GROD values in the HCP phase. More specifically, high GROD values were seen in both thermally- and deformation-induced HCP-martensites, and the GROD values were not uniform in HCP and some of them were higher than in FCC. This fact indicated that plastic deformation occurred significantly in HCP-martensite in the present HEA.

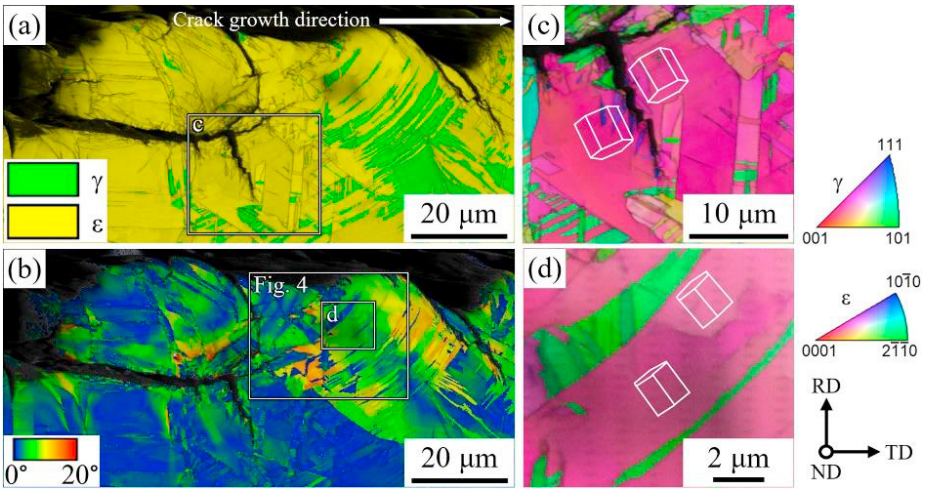

Fig. 3. EBSD images beneath the fracture surface of the HEA at ΔK of 18 MPa·m$^{1/2}$: (a) phase map; (b) grain reference orientation deviation (GROD) map; (c, d) rolling direction-inverse pole figure (RD-IPF).

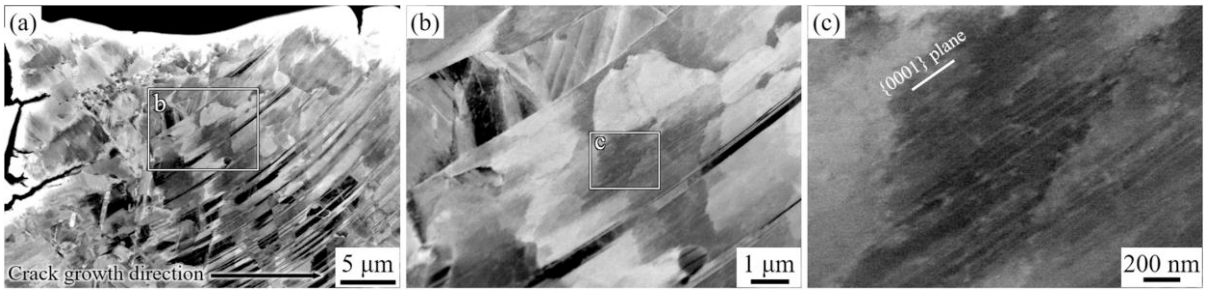

Fig. 4. ECC images beneath the fracture surface of the HEA at ΔK of 18 MPa·m$^{1/2}$. The RD-IPF corresponding to the region (b) is shown in Fig. 3d.

Another important finding was that the deformation of HCP phase was not associated with deformation twinning. It can be seen in Figs. 3c and 3d (RD-IPF) that the crystal orientation within HCP region was rather uniform, and twin boundaries were not recognized. In contrast, Li et al. (2017) reported from the tensile tests of Fe30Mn10Cr10Co HEA that deformation twins were intensively observed and twinning was an important deformation mechanism of the HCP phase. These facts indicated that the deformation mechanisms of HCP phase in the fatigue test were different from those in the tensile test. In high-Mn austenitic steels, microstructure evolution during fatigue tests is different from that during tensile tests (Niendrof et al., 2010, Shao et al., 2016). It is interesting to note that Fe22Mn0.6C (mass%) twinning-induced plasticity steel did not reveal twinning under cyclic loading, even though twinning was the main deformation mode in the case of tensile deformation (Niendrof et al., 2010). These results suggested that twinning was difficult during fatigue deformation irrespective of HCP or FCC phase.

For detailed discussion, we performed ECCI analysis beneath the fracture surface in HEA. Fig. 4 shows ECC images of the rectangular region indicated in Fig. 3b. The HCP-martensite region contained a significant orientation gradient (Fig. 4a), a cell-like structure (Fig. 4b), and a high density of dislocations and stacking faults (Fig. 4c). This is direct evidence for the activity of dislocation slip as the origin of high plastic deformability of HCP-martensite in HEA. Stacking faults were evidently associated with the operation of the basal plane slip system. Since cell formation normally needs operation of more than two slip systems (Bay et al., 1992), non-basal plane slip systems probably operated in the HCP-martensite. It is clear from the orientation information in Fig. 3d that the basal slip planes, namely stacking fault planes shown in Fig. 4c, were very close to an edge-on condition. With this fact, it should be noted that the length of individual dislocations in Fig. 4c was longer than the thickness of stacking faults, indicating that these dislocations were lying on non-basal slip planes. Thus, the operation of multiple slip systems including non-basal slip systems was evident in the HCP-martensite in HEA, even though we need further study to clarify the slip systems actually activated.

Here, we would like to make a few comments on the formation mechanisms of secondary cracks shown in Fig. 3. First, the secondary cracks were surrounded by HCP-martensite (Fig. 3a). Since the secondary cracks were observed within the blocky HCP-martensite region, it was clear that secondary cracking occurred in thermally-induced martensite. Second, the HCP portions near the secondary cracks showed higher GROD values (Fig. 3b), indicating that the secondary cracks were ductile and stemmed from slip localization. Third, Fig. 3c shows that the surface facets of secondary cracks were not parallel to both basal and prismatic planes, suggesting a kind of complicated slip deformation and damage accumulation as the origin of secondary cracking (Man et al., 2009, Hamada et al., 2018).

Finally, we would like to emphasize the significant plastic deformability of HCP-martensite in HEA. In conventional metastable austenitic steels (low-entropy alloys), HCP-martensite is cracked easily because of the small number of slip systems (Koyama et al., 2015, Ju et al., 2017). This negative effect of HCP-martensite enhances the fatigue crack growth rate. However, the present study showed that the HCP-martensite in HEA has multiple slip systems that lead to high plastic deformability, preventing the negative effect of HCP-martensite in the fatigue crack growth rate of HEA.

4. Conclusions

We investigated the fatigue crack growth behaviors of metastable Fe30Mn10Cr10Co HEA with FCC/HCP phases and 316L austenitic steel with stable FCC phase, paying special attention to the plastic deformability of HCP-martensite in HEA. The following conclusions were drawn:

- The crack growth rate of HEA was comparable to that of the 316L austenitic steel. The fatigue crack of HEA propagated smoothly, indicating that the crack propagation mode was mainly a mode I type like in 316L.
- Plastic deformation of mode I crack propagation was significantly caused by slip deformation in HCP-martensite in HEA. Twinning did not occur in HCP-martensite under fatigue deformation, unlike significant twinning under tensile deformation.
- In general, cracking occurs easily in HCP-martensite in low-entropy alloys because of the limited number of slip systems. However, cracking was difficult in the HCP-martensite in the present HEA owing to the operation of multiple slip systems leading to high plastic deformability.

Acknowledgements

This work was financially supported by JSPS KAKENHI (JP16H06365 and JP17H04956) and the support is greatly appreciated.

References

American Society for Testing and Materials (ASTM) International, 2011. Standard Test Method for Measurement of Fatigue Crack Growth Rates. ASTM standard E647.

Bay, B., Hansen, N., Hughes, D. A., Khulmann-Wilsdorf, D., 1992. Overview no. 96 evolution of f.c.c. deformation structures in polyslip. Acta Metall. Mater. 40, 205–219.

Hamada, S., Fukudome, S., Koyama, M., Ueda, M., Noguchi, H., 2018. Phenomenon and mechanism of fatigue crack propagation under Mode II loading: An example of cold rolled sheet steel. International Journal of Fatigue, submitted for publication.

Ichii, K., Koyama, M., Tasan, C.C., Tsuzaki, K., 2018. Comparative study of hydrogen embrittlement in stable and metastable high-entropy alloys. Scr. Mater. 150, 74–77.

Ju, Y.B., Koyama, M., Sawaguchi, T., Tsuzaki, K., Noguchi, H., 2017. Effects of ε-martensitic transformation on crack tip deformation, plastic damage accumulation, and slip plane cracking associated with low-cycle fatigue crack growth. Int. J. Fatigue 103, 533–545.

Koyama, M., Eguchi, T., Ichii, K., Tsuzaki, K., 2018. A new design concept for prevention of hydrogen-induced mechanical degradation: viewpoints of metastability and high entropy. To be published in the proceedings of ECF22.

Koyama, M., Sawaguchi, T., Ogawa, K., Kikuchi, T., Murakami, M., 2008. The effects of thermomechanical training treatment on the deformation characteristics of Fe-Mn-Si-Al alloys. Mater. Sci. Eng. A 497, 353–357.

Koyama, M., Sawaguchi, T., Tsuzaki, K., 2015. Effects of Si on tensile properties associated with deformation-induced ε-martensitic transformation in high Mn austenitic alloys. Nippon Kinzoku Gakkaishi/Journal Japan Inst. Met. 79, 657–663.

Li, Z., Pradeep, K.G., Deng, Y., Raabe, D., Tasan, C.C., 2016. Metastable high-entropy dual-phase alloys overcome the strength-ductility trade-off. Nature 534, 227–230.

Li, Z., Tasan, C.C., Pradeep, K.G., Raabe, D., 2017. A TRIP-assisted dual-phase high-entropy alloy: Grain size and phase fraction effects on deformation behavior. Acta Mater. 131, 323–335.

Man, J., Obrtlík, K., Polák, J., 2009. Extrusions and intrusions in fatigued metals. Part 1. State of the art and history. Philos. Mag. 89, 1295–1336.

Niendorf, T., Rubitschek, F., Maier, H.J., Niendorf, J., Richard, H.A., Frehn, A., 2010. Fatigue crack growth-Microstructure relationships in a high-manganese austenitic TWIP steel. Mater. Sci. Eng. A 527, 2412–2417.

Nikulin, I., Sawaguchi, T., Tsuzaki, K., 2013. Effect of alloying composition on low-cycle fatigue properties and microstructure of Fe-30Mn-(6-x)Si-xAl TRIP/TWIP alloys. Mater. Sci. Eng. A 587, 192–200.

Shao, C.W., Zhang, P., Liu, R., Zhang, Z.J., Pang, J.C., Duan, Q.Q., Zhang, Z.F., 2016. A remarkable improvement of low-cycle fatigue resistance of high-Mn austenitic TWIP alloys with similar tensile properties: Importance of slip mode. Acta Mater. 118, 196–212.

Takaki, S., Tadashi, F., Tokunaga, Y., 1990. Effect of Si and Al Additions on the Low Temperature Toughness and Fracture Mode of Fe-27Mn Alloys. ISIJ Int. 30, 632–638.